Electronic Supplementary Material (ESI) for Physical Chemistry Chemical Physics.

Solvent-mediated aggregate formation of PNDIT2: Decreasing the available conformational subspace by introducing locally highly ordered domains

— Supporting Information —

Deborah L. Meyer, Rukiya Matsidik, Sven Huettner, Michael Sommer, and Till Biskup*

Contents

*till.biskup@physchem.uni-freiburg.de

EPR Instrumentation

TREPR spectroscopy with a time resolution of up to 10 ns allows for real-time observation, *e.g.*, of short-lived radical-pair and triplet states generated by pulsed laser excitation. In contrast to conventional continuous-wave EPR spectroscopy, which usually involves magnetic-field modulation to improve the signal-to-noise ratio, TREPR is recorded in a high-bandwidth direct-detection mode, so as not to constrain the time resolution of the experiment. Consequently, positive and negative signal amplitudes in TREPR correspond to enhanced absorptive (A) and emissive (E) electron-spin polarisations of the EPR transitions, respectively.

All TREPR experiments were performed at 80 K using a commercial EPR spectrometer (Bruker ESP380E) in conjunction with a Bruker microwave bridge (ER 046 MRT) equipped with a low-noise high-bandwidth video amplifier. The sample was placed in a synthetic-quartz (Suprasil) sample tube (3 mm inner diameter) and irradiated in a dielectric-ring resonator (Bruker ER 4118X-MD5), which was immersed in a helium gas-flow cryostat (Oxford CF-935) cooled with liquid nitrogen. The temperature was regulated to ±0.1 K by a temperature controller (Oxford ITC-503). The time resolution of the experimental setup was in the 10 ns range. A microwave frequency counter (Hewlett-Packard HP 5352B) was used to monitor the microwave frequency.

Optical excitation at the respective wavelengths was carried out with an optical parametric oscillator (OPO) system (Opta BBO-355-vis/IR) pumped by an Nd:YAG laser (Spectra Physics, Quanta Ray GCR 190-10) with a pulse width of approximately 6 ns, and a pulse energy of 1 mJ. The repetition rate of the laser was set to 10 Hz. A transient recorder (LeCroy 9354A) with a digitizing rate of 2 ns/11 bit was used to acquire the time-dependent EPR signal. To eliminate the background signal induced by the laser entering the EPR cavity, TREPR signals were accumulated at off-resonance magnetic-field positions (background) and subtracted from those recorded on-resonance. This background signal is completely independent in its shape from both, laser wavelength and magnetic field, and normally long-lived compared to the detected spin-polarised EPR signal. Background subtraction was performed directly in the transient recorder and a background signal repeatedly recorded after each tenth time trace of the experimental data.

Further experimental parameters (except where explicity given) are as follows: Microwave frequency, 9.700 GHz, microwave power: 2 mW (20 dB attenuation, source power 200 mW), frequency-mixer detection, video amplifier set to 42 dB amplification and 25 MHz bandwidth, between 850 and 1400 averages per point.

TREPR spectra of triplet states

As TREPR spectra of spin-polarised triplet states of organic molecules recorded at X-band frequencies and magnetic fields are normally dominated by the zero-field splitting (ZFS) interaction, the hamilton operator used to describe the system reduces dramatically. The only contributions that need to be taken into account are the Hamilton operator for the Zeeman interaction, $\mathcal{H}_{\mathrm{EZ}}$, and the one for the ZFS interaction, $\mathcal{H}_{\mathrm{ZFS}}$:

$$\mathcal{H} = \mathcal{H}_{\mathrm{EZ}} + \mathcal{H}_{\mathrm{ZFS}} = \mathbf{g}\mu_{\mathrm{B}}\vec{S}\vec{B} + \vec{S}\mathbf{D}\vec{S}. \tag{S1}$$

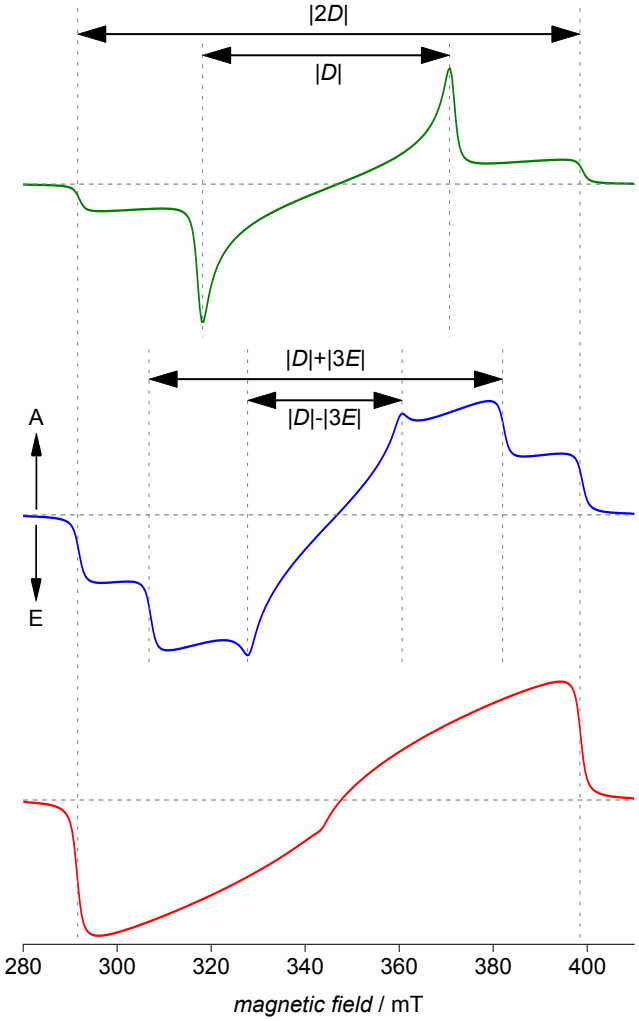

Figure S1: **Characteristics of TREPR spectra of (photo-generated) triplet states.** Three characteristic situations for the ratio of the two parameters D and E of the ZFS tensor are depicted here: the fully axial case (top, green), an intermediate case (blue, centre) and a fully rhombic case (red, bottom). Spectra were calculated using EasySpin. [2] The zero-field populations $p_{1,2,3}$ of the three triplet sublevels are far from thermal equilibrium, due to optical excitation and the inherent anisotropy of the intersystem crossing processes. Therefore, signals consist of both, absorptive (A) and emissive (E) contributions.

All other contributions can be considered as small perturbations that can be accounted for using (inhomogeneous) line broadening.

The **D** tensor in its principal axis system is given to

$$\mathbf{D} = \begin{pmatrix} -\frac{1}{3}D + E & 0 & 0 \\ 0 & -\frac{1}{3}D - E & 0 \\ 0 & 0 & \frac{2}{3}D \end{pmatrix} \tag{S2}$$

where D and E are the zero-field-splitting parameters that can be directly read out from the experimental spectra (cf. Fig. S1). Note that D and E are defined such in the simulation routine used that the relation $|E| \leq |D|/3$ always holds.

Spectral simulations of TREPR spectra of triplet states

All simulations of triplet spectra have been performed using the EasySpin software package [1] available for MATLAB® (MathWorks), and here the routine `pepper`. Parameters included were the **g** and **D** tensor and the triplet sublevel populations (in zero field). Line broadening (Γ) was included using a combination of Lorentzian (Γ_L) and Gaussian (Γ_G) lines. For all simulations, the **g** tensor was assumed to be isotropic, with $g_\mathrm{iso} = 2.002$, and the population p_1 was set to zero. This left the parameters D and E of the zero-field splitting tensor **D**, the populations p_2 and p_3, and the two line widths Γ_L and Γ_G as the only free parameters that were adjusted.

Fitting of the spectral simulations to the experimental data was done with the routine `lsqcurvefit` from the MATLAB® Optimization Toolbox™ using the trust-region-reflective least squares algorithm.

The nonlinear least-square solver finds the m coefficients $\vec{a}$ that solve the problem

$$\min_{\vec{a}} \sum_i (f(x_i;\vec{a}) - y_i)^2 \tag{S3}$$

with y_i being the measured data and $f(x_i;\vec{a})$ the fitting function $f : \mathbb{R}^m \to \mathbb{R}^n$ with the same size n as the measured data y_i

Error estimation of the fitting parameters was carried out by using the Jacobian matrix **J**. J_{ij} is the partial derivative of the fitting function $f(x_i;\vec{a})$ with respect to a_j at the solution a_0.

$$J_{ij}(\vec{a}_0) := \left(\frac{\partial f(x_i;\vec{a})}{\partial a_j}(\vec{a}_0) \right)_{i=1\ldots n, j=1\ldots m} \tag{S4}$$

$$\mathbf{J}(\vec{a}_0) = \begin{pmatrix} \frac{\partial f(x_1;\vec{a})}{\partial a_1}(\vec{a}_0) & \ldots & \frac{\partial f(x_1;\vec{a})}{\partial a_m}(\vec{a}_0) \\ \ldots & & \\ \frac{\partial f(x_n;\vec{a})}{\partial a_1}(\vec{a}_0) & \ldots & \frac{\partial f(x_n;\vec{a})}{\partial a_m}(\vec{a}_0) \end{pmatrix} \tag{S5}$$

The variances of the coefficients a_j are given by the diagonal elements of the covariance matrix, **C**, i.e. $\sigma_{a_j}^2 = C_{jj}$, where **C** is the inverse of the matrix **H**, variously referred to as the curvature or Hessian matrix.

The Hessian matrix was approximated by a series expansion, which is terminated after the first rank:

$$H_{jk} = \frac{1}{2}\frac{\partial^2 \chi^2(\vec{a})}{\partial a_j \partial a_k} \approx \sum_{i=1}^{n} \frac{1}{\sigma_i^2} \frac{\partial f(x_i;\vec{a})}{\partial a_j} \frac{\partial f(x_i;\vec{a})}{\partial a_k}$$

Hence the Jacobian matrix can be used to approximate the Hessian if σ_i^2 is chosen to be equal for all points,

$$\mathbf{H} \approx \frac{1}{\sigma_i^2}\, \mathbf{J}^T \cdot \mathbf{J}. \tag{S6}$$

To speed up calculation time for the matrix product $\mathbf{J}^T \cdot \mathbf{J}$, an economy-size QR decomposition of **J** was carried out, reducing the dimension of **R** to the size of $\vec{a}$:

$$\mathbf{J} = \mathbf{Q} \cdot \mathbf{R}. \tag{S7}$$

In the following matrix multiplication, $\mathbf{Q}$ vanishes by multiplication with $\mathbf{Q}^T$:

$$(\mathbf{J}^T \cdot \mathbf{J})^{-1} = (\mathbf{R}^T \cdot \mathbf{R})^{-1} = \mathbf{R}^{-1} \cdot (\mathbf{R}^T)^{-1} = \mathbf{R}^{-1} \cdot (\mathbf{R}^{-1})^T \tag{S8}$$

In MATLAB®, this implementation leads to high computational speed and only minor numerical errors. The corresponding code would be as follows:

```
[~,R] = qr(jacobian,0);
```

The diagonal elements of the approximated $\mathbf{H}^{-1}$ can easily be calculated by element-wise squaring followed by summation over the rows of $\mathbf{R}$. Since σ_i^2 is chosen to be equal for all points, the errors for the fit parameters are given by:

```
stdDev = sqrt(variance * sum(inv(R).^2,2));
```

The fitting algorithm `lsqcurvefit` can optionally return the residuals as additional output argument, here termed `residuals`. Hence the variance of the residuals obtained as

```
variance = var(residuals);
```

was used as σ^2 for all points.

Absorption spectra of PNDIT2-13k at different temperatures

For better comparison of optical and TREPR data, we recorded absorption spectra as well at lower temperatures (Fig. S2). Note, however, that 1-chloronaphthalene has a melting point of about 267 K and does not form a glass if frozen, therefore rendering absorption spectroscopy below the melting point impossible. Although cooling down still increases aggregate formation in toluene, the effect is much less pronounced as compared to PNDIT2-7k (see Fig. 3 in main text for comparison). However, no sign of aggregation can be observed in 1-chloronaphthalene.

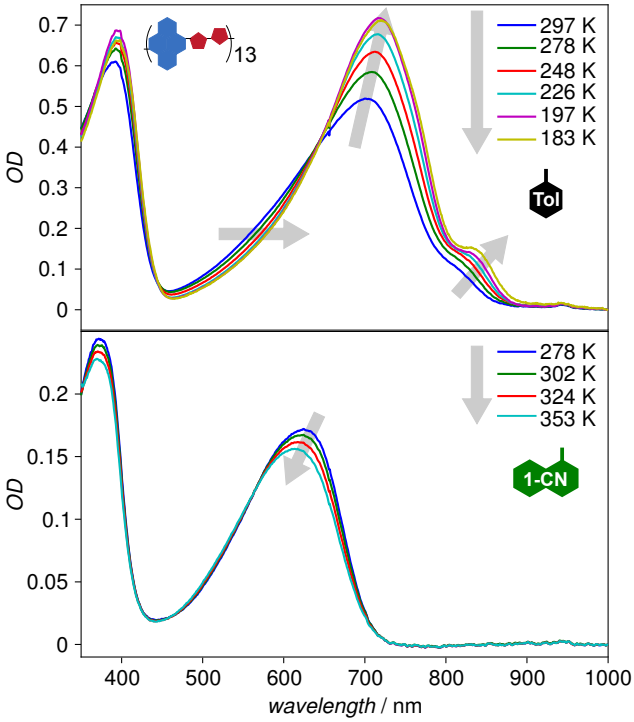

Figure S2: **Absorption spectra of PNDIT2-13k at different temperatures for better comparison with TREPR data.** Only the data for PNDIT2-13k are shown here, for both solvents, toluene and 1-chloronaphthalene. Although cooling down still increases aggregate formation in toluene, the effect is much less pronounced as compared to PNDIT2-7k (see Fig. 3 in main text for comparison). However, no effect can be observed in 1-chloronaphthalene. Note that 1-chloronaphthalene freezes already at about 267 K and does not form a glass, rendering absorption spectroscopy at lower temperatures impossible. For the corresponding measurements on PNDIT2-7k, cf. Fig. 3 in the main text.

TREPR signal decay and triplet lifetime

The kinetics of TREPR signals of triplet states are rather complicated, involving spin relaxation, decay of spin polarisation, and decay of the actual triplet state, usually via intersystem crossing back into the singlet ground state. Hence, only a lower limit of the triplet lifetime can be extracted from the TREPR time profiles, based on the simple fact that regardless of all other processes, TREPR signals will only be observable as long as there exists a triplet state.

As can be seen from the full 2D datasets of all four samples investigated in this study (Fig. S3), TREPR signals decay on the time scale of several microseconds. However, it is highly likely that

this decay is dominated by the microwave power and other experimental parameters and that the actual triplet state lifetime extends well into tens or even hundreds of microseconds.

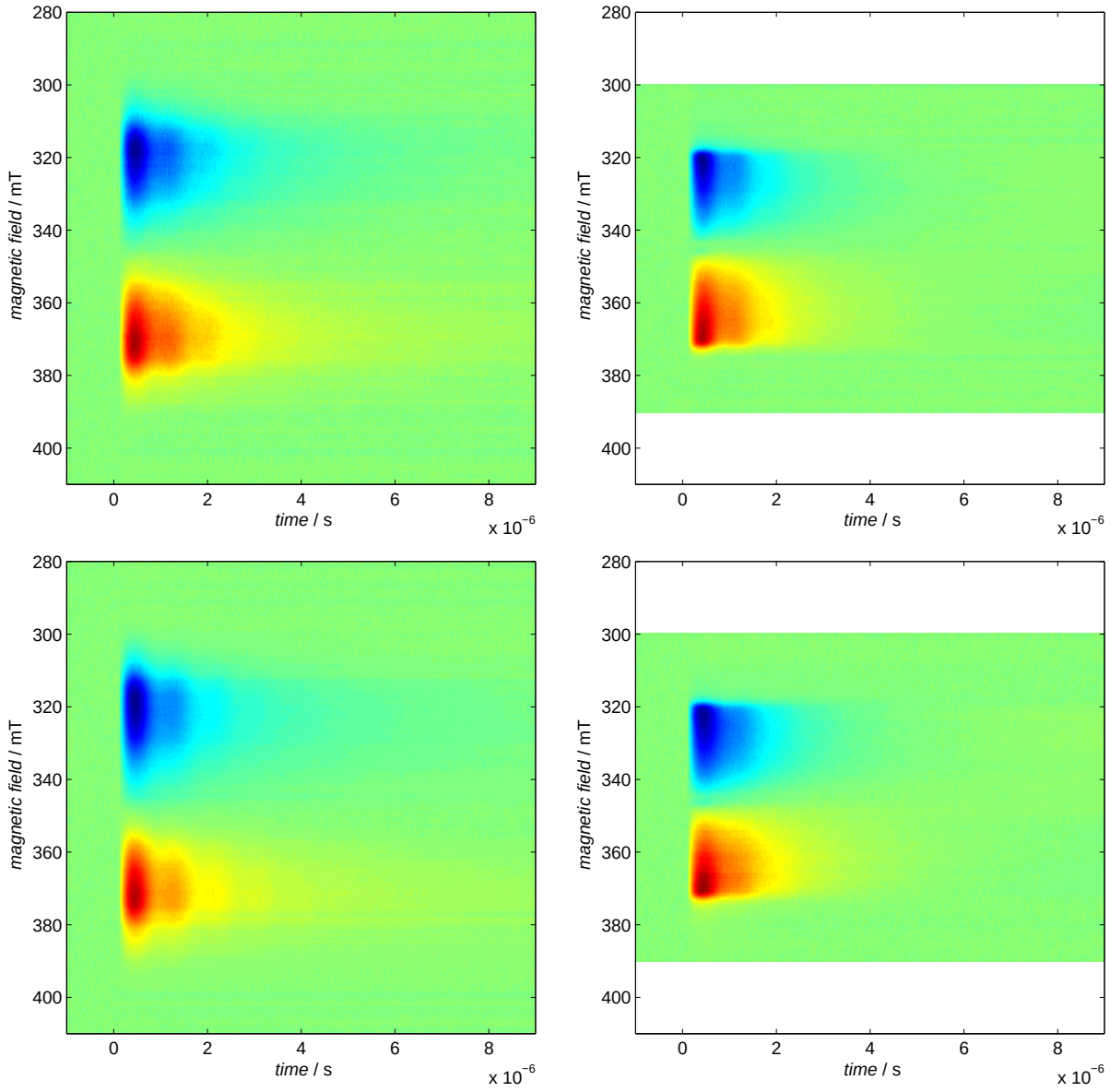

Figure S3: **Full 2D TREPR datasets of all four samples investigated in this study.** Left: 1-chloronaphthalene, right: toluene; top: PNDIT2-7k, bottom: PNDIT2-13k. Blue: emissive, red: enhanced absorptive polarisation. For experimental details see main text.

Comparison of TREPR spectra on frozen solution and thin film

For better visibility, in the main text only the spectra of PNDIT2 drop-cast on quartz glass substrate in comparison with the spectra obtained in frozen solution have been shown and the results of the simulations summarised.

Here, we present a detailed overview of all four spectra with accompanying simulations (Fig. S4) together with the simulation parameters obtained (Tab. S1). To account for the preferential orientation of the molecules in thin film, an ordering parameter has been used. Positive values of this ordering parameter denote systems with molecules preferentially oriented with their z axis collinear to the external magnetic field, negative values denote systems with molecules preferentially oriented with their z axis perpendicular to the external magnetic field.

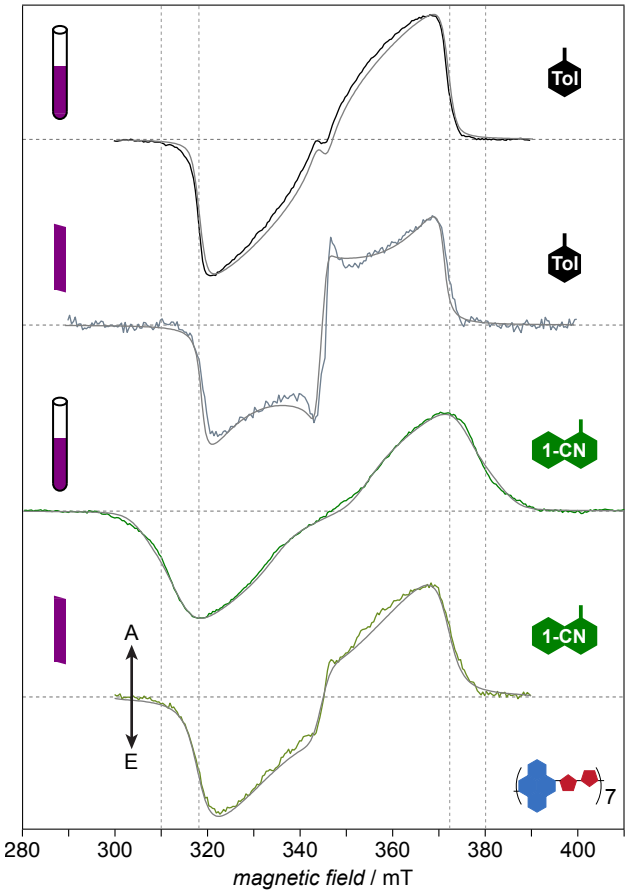

Figure S4: **Comparison of the TREPR spectra of PNDIT2 in toluene for frozen solution and drop-cast on glass substrate.** Note that the overall shape and width of both spectra are rather similar, pointing towards an equally similar degree of delocalisation of the triplet exciton.

References

[1] Stefan Stoll and Arthur Schweiger. EasySpin, a comprehensive software package for spectral simulation and analysis in EPR. *J. Magn. Reson.*, 178:42–55, 2006.

Table S1: **Simulation parameters for the spectral simulations shown in Fig. S4.** D and E are the parameters of the zero-field splitting tensor of the dipolar interaction, Γ_{G} is the Gaussian, Γ_{L} the Lorentzian line width, and $p_{1,2,3}$ are the populations of the three triplet sublevels, respectively. Ordering is a parameter necessary to account for the highly ordered spectra obtained from thin films drop-cast on quartz glass.

Preparation	Solvent	D/mT	E/mT	Γ_{G}/mT	Γ_{L}/mT	$p_{1,2,3}$	Ordering
solution	Tol	765 ± 1.2	244 ± 0.7	2.0 ± 0.3	1.2 ± 0.1	$0, 0, 1$	–
film	Tol	770 ± 4.2	233 ± 1.2	$0.5 \pm \mathrm{NaN}$	1.9 ± 0.1	$0, 0.47, 0.53$	-4.4 ± 0.4
solution	1-CN	1079 ± 3.6	228 ± 2.0	6.8 ± 0.5	1.5 ± 0.4	$0, 0.23, 0.77$	–
film	1-CN	755 ± 8.3	237 ± 18.1	2.6 ± 0.7	4.1 ± 0.3	$0, 0.71, 0.29$	0.3 ± 0.3